scientific reports

Check for updates

OPEN

Computational investigation of IP_3 diffusion

Roberto Ornelas-Guevara[1], Diana Gil[2], Valérie Voorsluijs[3] & Geneviève Dupont[1]✉

Inositol 1,4,5-trisphosphate (IP_3) plays a key role in calcium signaling. After stimulation, it diffuses from the plasma membrane where it is produced to the endoplasmic reticulum where its receptors are localized. Based on in vitro measurements, IP_3 was long thought to be a global messenger characterized by a diffusion coefficient of ~ 280 $\mu m^2 s^{-1}$. However, in vivo observations revealed that this value does not match with the timing of localized Ca^{2+} increases induced by the confined release of a non-metabolizable IP_3 analog. A theoretical analysis of these data concluded that in intact cells diffusion of IP_3 is strongly hindered, leading to a 30-fold reduction of the diffusion coefficient. Here, we performed a new computational analysis of the same observations using a stochastic model of Ca^{2+} puffs. Our simulations concluded that the value of the effective IP_3 diffusion coefficient is close to 100 $\mu m^2 s^{-1}$. Such moderate reduction with respect to in vitro estimations quantitatively agrees with a buffering effect by non-fully bound inactive IP_3 receptors. The model also reveals that IP_3 spreading is not much affected by the endoplasmic reticulum, which represents an obstacle to the free displacement of molecules, but can be significantly increased in cells displaying elongated, 1-dimensional like geometries.

Within all cell types, Ca^{2+} signaling is controlled by a variety of channels and pumps that allow for rapid and highly regulated Ca^{2+} fluxes at specific locations of the cell[1]. In many instances, Ca^{2+} increases are initiated by the formation of inositol 1,4,5-trisphosphate (IP_3) at the plasma membrane[2]. IP_3 diffuses in the cytoplasm and binds its receptors located on the endoplasmic reticulum that contains a large quantity[3] of rapidly mobilizable Ca^{2+}. Activity of these receptors is also regulated by cytosolic Ca^{2+}, both positively and negatively[4]. At the spatial level, IP_3 receptors (IP_3R) are not homogeneously scattered on the ER membrane, but rather grouped in clusters of ~ 10–20 channels[5,6]. Because the number of clusters in cells is limited, coupling between clusters has been much investigated to understand how Ca^{2+} signaling can be coordinated at the cellular level, giving rise to Ca^{2+} oscillations and waves[7–9]. Most studies have focused on Ca^{2+}-mediated communication between clusters, since it was assumed that all clusters rapidly experience the increase of IP_3 that results from the stimulation of the cell. In cytosolic extracts of *Xenopus* oocytes, apparent diffusion coefficients of Ca^{2+} and IP_3 indeed equal 38 ± 11 $\mu m^2 s^{-1}$ and 283 ± 53 $\mu m^2 s^{-1}$, respectively[10]. Considering in addition the respective rates of Ca^{2+} removal from the cytoplasm and IP_3 metabolism, these values led Allbritton et al.[10] to conclude that Ca^{2+} mostly acts in restricted domains and that IP_3 is a global messenger.

The notion that IP_3 acts as a global messenger was however contradicted by indirect in vivo observations[11]. To evaluate the rate at which IP_3 diffuses in an intact cell, the group of Ian Parker used the IP_3-evoked liberation of Ca^{2+} from a cluster of IP_3Rs as a detector of the presence of IP_3 at the cluster location. Such Ca^{2+} increases evoked by clusters of IP_3Rs are well-known as Ca^{2+} puffs[12]. If a non-metabolizable IP_3 analog is released at one extremity of an elongated SH-SY5Y cell, the time lapse between the localized IP_3 increase and the occurrence of the first Ca^{2+} puff significantly increases with the distance between the spot of IP_3 release and the location of Ca^{2+} rise. This time lapse, called *latency*, reflects the time taken by IP_3 to diffuse on this distance. Accordingly, when the IP_3 analog is uniformly released across the entire cell, latency does not show any systematic variation along the cell length but decreases with increasing IP_3 concentration. The fact that latency increases with the distance from the IP_3 release spot clearly indicates that IP_3 does not act as a global messenger in these conditions. From these observations, Dickinson et al.[11] inferred the value of the IP_3 diffusion coefficient by resorting to a simplified mathematical expression for the probability of Ca^{2+} puff occurrence coupled to 1-dimensional (1D) simulations of IP_3 diffusion. These calculations predicted an effective IP_3 diffusion coefficient lower than 10 $\mu m^2 s^{-1}$, *i.e.* about 30 times slower than in vitro estimations.

[1]Unité de Chronobiologie Théorique, Faculté Des Sciences, Université Libre de Bruxelles (ULB), Boulevard du Triomphe, CP231 Brussels, Belgium. [2]The Calcium Signalling Group, Department of Biochemistry and Molecular Cell Biology, University Medical Center Hamburg Eppendorf, Hamburg, Germany. [3]Luxembourg Centre for Systems Biomedecine, Université du Luxembourg, Esch-sur-Alzette, Luxemburg. ✉email: Genevieve.Dupont@ulb.be

This slowing down of IP_3 diffusion within cells as compared to cytosolic extracts was ascribed to the presence of IP_3Rs that are not fully bound to IP_3[11,13]. IP_3Rs are indeed tetramers that release Ca^{2+} only when each IP_3R monomer is occupied by IP_3[14]. Given that IP_3 binding on IP_3Rs is not cooperative, most of the receptors are partially bound as long as $[IP_3]$ remains lower than the K_D of IP_3 binding, *i.e.* ~ 100 nM (K_D = 119 nM reported by Taylor and Konieczny[13]) and thus act as a buffer of IP_3. Assuming fast binding and unbinding of IP_3 to and from its receptor, the resulting effective diffusion coefficient[15] is given by:

$$D_I = \frac{D}{1+R}, \quad \text{with} \quad R = \frac{S_T.K_D}{(K_D + [IP_3])^2}, \tag{1}$$

where D represents the IP_3 diffusion coefficient in the absence of buffers, S_T the concentration of IP_3R monomers, and K_D the equilibrium dissociation constant of IP_3 from its receptor. S_T is cell dependent, in the range of 80 nM to 2 µM[13,16–18] with an estimated value of 542 nM in SH-SY5Y cells[18]. Thus, the buffering effect described by Eq. 1 is expected to induce a reduction of the effective diffusion coefficient of ~ 2.25 at $[IP_3] = K_D$. In Dickinson et al.[11] experiments, $[IP_3]$ was in the Ca^{2+} oscillatory range. Because IP_3 concentrations are typically of the order or lower than the K_D of the IP_3R in the oscillatory range[19], one can estimate that the effective diffusion coefficient of IP_3 considering IP_3 buffering by not fully bound receptors (D_I) should be ~ 100 $\mu m^2 s^{-1}$ (Fig. 1). Values around 5–10 $\mu m^2 s^{-1}$ would correspond to situations in which IP_3 concentrations are lower than $K_D/2$ and IP_3R concentrations at least higher than 1 µM, in which IP_3 binding to its receptors exceeds what occurs in SH-SY5Y cells. Such discrepancy led Dickinson et al.[11] to hypothesize the existence of two distinct populations of IP_3Rs, with the most active exhibiting different binding and/or gating properties. These different populations were proposed to be the molecular bases of the observed two modes of Ca^{2+} release: one early pulsatile Ca^{2+} activity at puff sites and one later, spatially more diffuse Ca^{2+} liberation[20].

Besides, a value of D_I lower than 10 $\mu m^2 s^{-1}$ raises questions about some observations related to Ca^{2+} waves. For example, in ascidian eggs that have a radius between 25 and 38 µm, Ca^{2+} waves propagate across the entire fertilized egg in less than 10 s while IP_3 is only synthesized at the plasma membrane[21]. The question is even more critical for intercellular Ca^{2+} waves, which in many cases rely on the propagation of IP_3 through gap junctions[22]. Intracellular diffusion of IP_3 with a coefficient ≤ 10 $\mu m^2 s^{-1}$ could not account for waves propagating at rates ≥ 10 $\mu m s^{-1}$ among a cell population[23,24]. More generally, an accurate quantitative description of IP_3 diffusion is necessary for the numerous modelling studies devoted to the physiological responses induced by IP_3-controlled Ca^{2+} signaling, such as, for example, the Ca^{2+}- and IP_3-regulated nitric oxide production in neurons[25], the metabolism of β-amyloids during the development of Alzheimer's disease[26] or salivary secretion by acinar cells[27]. IP_3 spreading from its location of synthesis to its receptors also plays a key role in cardiac cells[28,29].

The aim of the present study is to re-investigate the characteristics of IP_3 diffusion using a stochastic model that explicitly simulates Ca^{2+} puff dynamics and allows a realistic computational description of the experiments performed by Dickinson et al.[11]. Based on the observations of puff latencies performed by these authors, we propose a new computational treatment to infer the value of the effective diffusion coefficient of IP_3, leading to different conclusions. The reasons for the different outcomes between the two studies are analyzed in the discussion. We also investigate how cell geometry and the presence of the ER membranes, which provide an obstacle to the free displacement of molecules, affect the rates at which IP_3 diffuses in a cell-like environment.

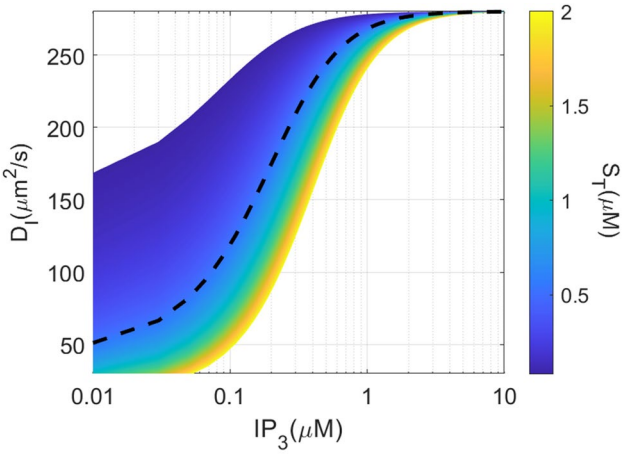

Figure 1. Theoretical values of the effective IP_3 diffusion coefficient depending on the concentration of IP_3 and of the monomers of IP_3 receptors (S_T). The dashed line shows this diffusion coefficient as a function of $[IP_3]$ for S_T = 542 nM, which is the value estimated for SH-S5Y5 neuroblastoma cells. Values have been calculated using Eq. 1. See text for details.

Results

Methodology. We performed explicit stochastic simulations of Ca^{2+}[14] releasing activities of puff sites located at different distances from an IP_3 source, in order to directly simulate the experimental protocol that was used to estimate the IP_3 diffusion coefficient *in vivo*[11]. The mathematical model is based on a previously proposed fully stochastic description of the Ca^{2+} exchanges between the ER and the cytosol via IP_3Rs, SERCA pumps and a leak from the ER[9]. In this work, SERCA pumps, Ca^{2+} leakage and Ca^{2+} diffusion are described deterministically. The effective value of the Ca^{2+} diffusion coefficient taking Ca^{2+} buffering into account[10] is considered, *i.e.* 40 $\mu m^2 s^{-1}$. To simulate Ca^{2+} puffs, the release of Ca^{2+} via the IP_3Rs is described stochastically, using the Gillespie's algorithm[30]. Each cluster of IP_3Rs (Supplemental Figure S1) is described as a whole and can be in four states: one open (O), one closed (C) and two different inhibited ones (I_1 and I_2). These states describe the global behavior of a cluster composed of close-by IP_3Rs. The phenomenological model was shown to reproduce experimentally observed statistical properties of Ca^{2+} puffs[31] and to describe the passage from localized puffs to global Ca^{2+} spikes when clusters are effectively coupled by Ca^{2+} diffusion[9].

To evaluate the effective diffusion coefficient of IP_3, this model is extended to take the dependence of puff occurrence on IP_3 concentration into account. Thus, in the Gillespie's simulations, the propensity of transition of the cluster from the closed (C) to the open (O) state now writes:

$$P_{C\to O} = k_{CO}\frac{N_{Ca}}{\Omega}\left(\frac{N_{IP}}{N_{IP}+K_{IP}}\right)^4, \tag{2}$$

where k_{CO} stands for the rate constant that characterizes the passage of the cluster from the closed to the open state, N_{Ca} is the number of cytosolic Ca^{2+} ions and Ω is the extensivity parameter. N_{IP} and K_{IP} represent the number of IP_3 molecules and the IP_3 dissociation constant of the IP_3R (multiplied by Ω), respectively. Although the model does not simulate individual IP_3 receptors, we assumed that puff firing probability is related to the probability of one tetrameric IP_3R to be fully bound to IP_3[13]. As shown below, Eq. 2 indeed allows to reproduce the exponential dependence of mean first puff latency on IP_3 concentration reported experimentally[11,32].

The evolution of IP_3 concentration is described deterministically and two different protocols of photorelease of caged IP_3 are simulated. The first one corresponds to a spot photorelease of caged IP_3 in a small region of the cell:

$$\frac{\partial[IP_3]}{\partial t} = D_I\nabla^2[IP_3] + \theta H\left(t_{ph}-t\right) \quad \text{at the location of the flash,} \tag{3}$$

$$\frac{\partial[IP_3]}{\partial t} = D_I\nabla^2[IP_3] \quad \text{everywhere else.} \tag{4}$$

In the second one, called "distributed photorelease", IP_3 is liberated at different spots to get an increase in $[IP_3]$ that is nearly spatially homogeneous in the whole cell. In this case:

$$\frac{\partial[IP_3]}{\partial t} = D_I\nabla^2[IP_3] + \left(\frac{\theta}{10}\right)H\left(t_{ph}-t\right) \quad \text{at the 10 locations of the flash,} \tag{5}$$

$$\frac{\partial[IP_3]}{\partial t} = D_I\nabla^2[IP_3] \quad \text{everywhere else.} \tag{6}$$

In Eqs. (3–6), D_I stands for the effective IP_3 diffusion coefficient, θ for the rate of IP_3 release upon laser flash and H for Heaviside function. This function equals 1 if $t \le t_{ph}$ and 0 otherwise. Considering that θ is determined by the intensity of the flash in the spot photorelease case (Eq. 3), a ten times smaller value is used to simulate distributed photorelease (Eq. 5) because the same total amount of IP_3 is distributed among the ten IP_3 releasing sites. Basal IP_3 concentration is set to 50 nM[33].

A detailed description of the algorithm is provided in the Supplementary Information (Sect. 1), together with a Table listing the propensities used for the stochastic part of the algorithm and the evolution equations used in the deterministic part (Table Supplement 1). Code are available at https://github.com/RobertoOrnelasGuevara/ca2-puffs/tree/main. Except for the process describing IP_3 dynamics listed here above, the values of parameters are taken from Voorsluijs et al.[9] and are listed in Table Supplement 2.

Validation of the model. Low concentrations of IP_3 typically evoke local Ca^{2+} signals known as Ca^{2+} puffs[12,34]. As the concentration of IP_3 increases, Ca^{2+} puffs become more frequent and transform into Ca^{2+} waves spreading regeneratively across the cell. These repetitive waves, also known as Ca^{2+} spikes, are more regular than puffs and are often referred to as Ca^{2+} oscillations. Their stochastic origin is visible by the linear relation between the variance on the interspike interval and the mean interspike interval itself[8,35]. In experiments, Ca^{2+} waves propagation can be hindered by loading the cells with the slow Ca^{2+} buffer EGTA, which reduces communication between puff sites[36]. At high EGTA concentrations, each cluster practically behaves as an independent entity and thus generates Ca^{2+} puffs on a large range of $[IP_3]$.

Such behavior is well reproduced by the stochastic model, as seen by simulations in a simplified 2D geometry (Fig. 2A–D). Four different conditions were used: low and intermediate IP_3 concentration, with and without coupling between clusters by Ca^{2+} diffusion. In all cases, $[IP_3]$ is constant in time and space. To model puff dynamics when clusters are uncoupled (corresponding to the presence of EGTA), a single cluster was simulated and the local Ca^{2+} concentration averaged in 1fL around the cluster was monitored. The resulting dynamics of $[Ca^{2+}]$ (Fig. 2A,B) corresponds to Ca^{2+} puffs, with statistical properties in good agreement with observations and an

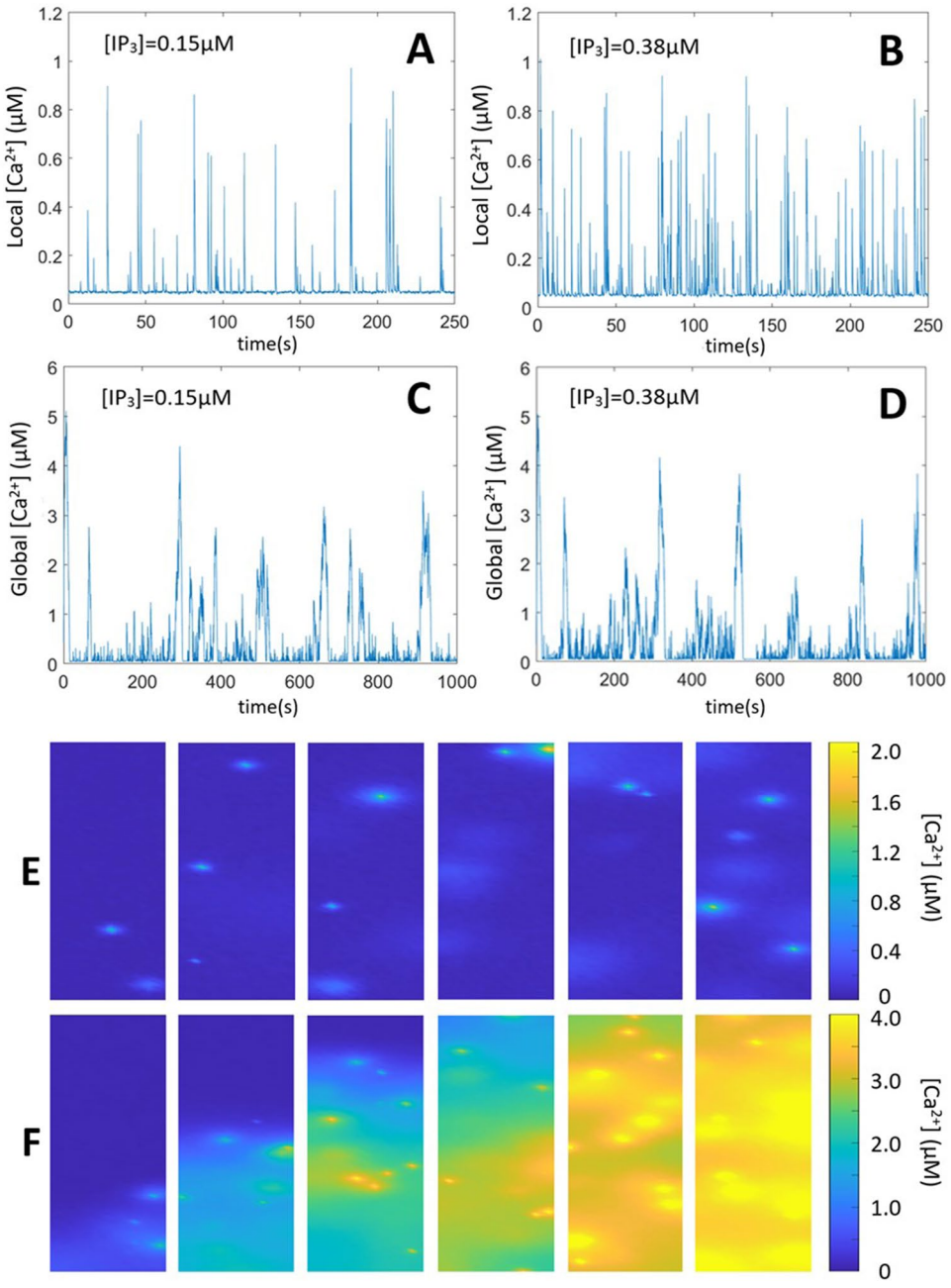

Figure 2. Stochastic simulations of Ca^{2+} puffs and spikes. (**A and B)** show the evolution of Ca^{2+} concentration in a 1 fL volume (1.5×1.5 μm^2 in the 2D simulations, see Voorsluijs et al.[9]) centered around the cluster at two [IP_3]. For the 2 panels, one cluster, located at the centre of a 5×5 μm^2 2D system is considered. For panels (**C and D)**, a larger 5×10 μm^2 system containing 10 clusters is simulated. All values of parameters are the same as in A and B and listed in Table S2. Time series show the evolution of Ca^{2+} concentration averaged on the whole system. Panels (**E and F)** show the spatio-temporal evolutions of Ca^{2+} puffs and spikes, respectively. In the two cases, the system is 50×10 μm^2 large and 10% of the total surface is occupied by clusters (200 clusters). For panel E, [IP_3] is constant and equal to 0.075 μM everywhere in the cell. For panel F, IP_3 was released in one spot (with dimensions 0.5×0.5 μm^2) located in the bottom center of the simulated cell. For panels E and F, times corresponding to each subpanels are: 0.1, 0.6, 2.5, 3.4 and 5.2 s after the increase in [IP_3] from 10 nM. In panels A-E, [IP_3] is increased at time 0, and Eqs. (3) and (5) are not considered. In panel F, the release of IP_3 is simulated using Eq. (3), with $\theta = 1000 \mu M s^{-1}$, $D_I = 100$ μm^{2}s^{-1} and $t_{ph} = 500$ ms.

average inter-puffs interval that decreases with [IP_3][9]. The mean interpuff intervals are 4.60 ± 4.25 s and 1.86 ± 1.79 at 0.15 μM and 0.38 μM [IP_3], respectively. Thus, the model recovers the characteristic stochastic activity of

an isolated cluster of IP_3Rs. To model spikes dynamics when clusters are coupled by diffusion, 10 clusters of IP_3Rs were randomly distributed in a 5 μm × 5 μm system and the global $[Ca^{2+}]$ averaged over the whole system was monitored (Fig. 2C,D). The mean interspike interval and the coefficient of variation (CV) decrease when increasing $[IP_3]$, as reported previously[35]: the mean interspike intervals are 129.6 ± 64.00 s and 108.26 ± 49.22 s at 0.15 μM and 0.38 μM $[IP_3]$, respectively. This exemplifies that global, more regular Ca^{2+} increases occur when clusters communicate via Ca^{2+} diffusion. To simulate the spatio-temporal profiles of puffs and spikes, simulations were performed in a 50 μm × 10 μm system, while keeping the same average density of clusters (Fig. 2E,F). While a low, homogeneous concentration of IP_3 induces random puff activity, a large bolus of IP_3 released at one extremity of the cell initiates a global Ca^{2+} spike that propagates as a Ca^{2+} wave.

Upon a spatially uniform increase in IP_3 concentration, latencies of first puff occurrence are exponentially distributed[12,32]. Such distributions, obtained by model simulations, are shown in Fig. 3A–C, together with their means and associated standard error of the mean (SEM) values. First puff latencies are exponentially distributed with an average that decreases with the IP_3 concentration, consistent with observations in SH-SY5Y cells[11]. The characteristic decrease times of the exponential distributions (τ) also decrease with $[IP_3]$. These results were used to infer the values of the rate of release of caged IP_3 in response to the flash, *i.e.* the value of parameter θ in Eqs. 3 and 5. Starting from the relation between mean first puff latency and flash duration reported by Dickinson et al.[11] for the distributed photorelease of IP_3 -and replotted in Fig. 3D, we seek the values of IP_3 concentrations that, in

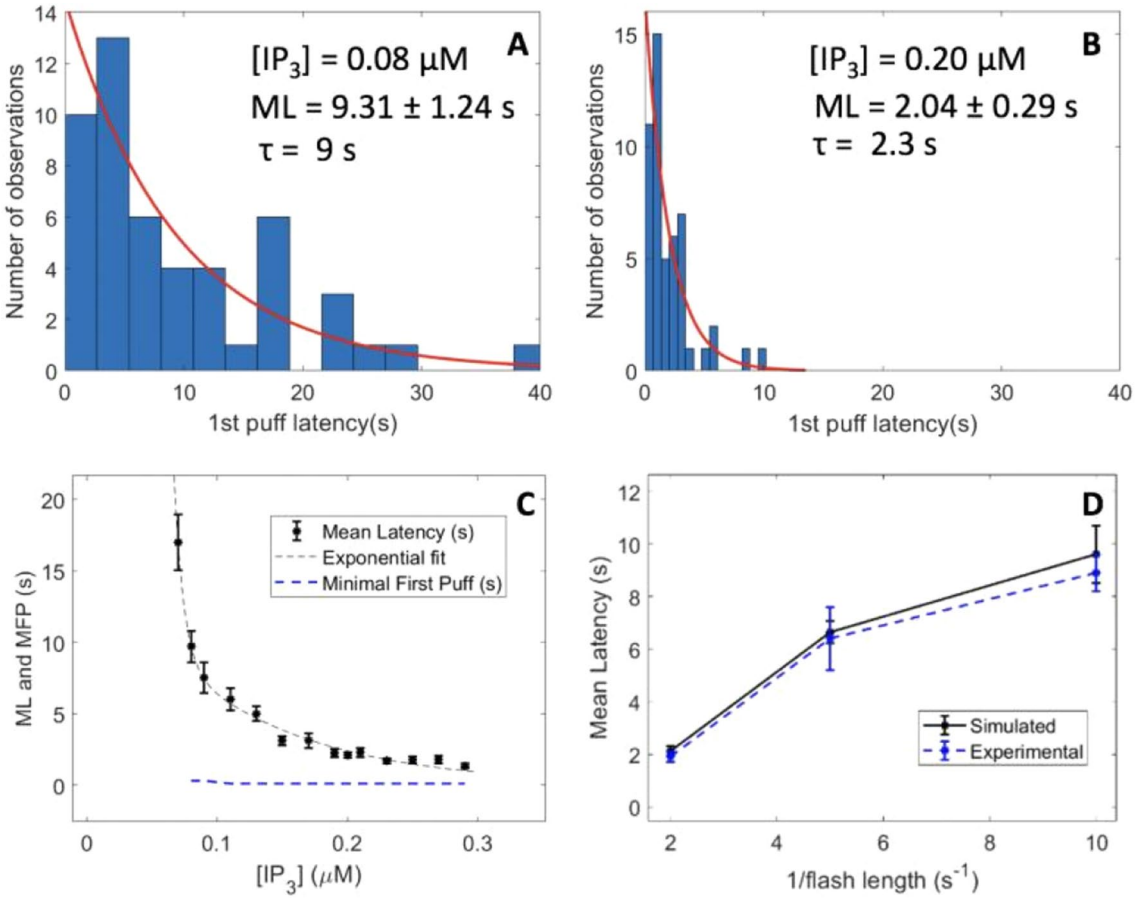

Figure 3. Statistics of the latencies of first puffs simulated with the model. Panels (**A and B)** show histograms of first puff latencies resulting from simulations of one cluster site in a square $5 \times 5 \mu m^2$ 2D geometry. A puff is defined as an increase in the cytosolic Ca^{2+} concentration in a 1 fL volume (1.5×1.5 μm^2 in the 2D simulations, see Voorsluijs et al.[9]) centered around the cluster that exceeds 0.1 μM. First puff latencies show an exponential distribution with characteristic decrease times matching experimental observations. Time t = 0 corresponds to the moment of $[IP_3]$ increase from 50 nM to indicated values. The black stars in panel **(C)** show the mean first puff latencies (ML) as a function of $[IP_3]$. The blue dashed line shows the minimal first puff latencies (MFP), *i.e.* the time at which the first puff occurred. Minimal first puffs are practically independent of $[IP_3]$ and are always close to 300 ms. For each $[IP_3]$, 50 independent simulations were run. In panels A, B and C, $[IP_3]$ is increased at time 0, and Eqs. (3) and (5) are not considered. In panel D, photorelease of caged IP_3 is also simulated, using Eq. (5). Best fit with the observations of Dickinson et al.[11] was found when considering $\theta = 600$ μMs^{-1}. This value was found by looking for the value of θ that allows to obtain the steady states $[IP_3]$ leading to the ML's corresponding to the flash durations (t_{ph}) used in Dickinson et al.'s experiments, i.e. 8.9 ± 0.5 s, 6.4 ± 1.2 s and 1.9 ± 0.2 s for the 0.1, 0.2 and 0.5 s flash durations, respectively. Error bars indicate ± SEM.

the simulations, gave the same mean latencies as those reported experimentally using Fig. 3C. Next, we numerically evaluated the value of θ allowing to reach these spatially uniform concentrations of IP_3 when assuming 10 photorelease spots of durations equal to 0.1, 0.2 and 0.5 s respectively, as in the experiments. Good agreement between mean latencies and flash durations was found for $\theta = 600$ µM/s (Fig. 3D).

When caged IP_3 is photoreleased at one extremity of the cell, puffs begin on average after longer latencies at greater distance from the spot[11]. This reflects the time taken for IP_3 to diffuse up to the cluster, and IP_3 dilution. Dickinson et al.[11] used mean first puff latencies at different distances from the photorelease spot to estimate the effective diffusion coefficient of IP_3. In addition to *mean* first puff latencies, the time interval between the flash and the observation of the first puff at a given distance from the release site is also a relevant quantity. We called this latency "*minimal* first puff latency". It can be regarded as the time lapse during which all clusters located at a given distance from the flash site remain silent, indicating that IP_3 diffusion up to this point has been negligible. As visible in the distribution of puff latencies upon a global IP_3 increase, the minimal first puff latency is shorter than 0.5 s as soon as $[IP_3]$ exceeds 80 nM (Fig. 3C, blue dashed line). In agreement with this, the minimal first puff latency is not affected by the duration of the flash in the case of distributed photorelease of IP_3[11]. If the source of IP_3 is spatially restricted, minimal first puff latency provides a reliable indication of the time at which IP_3 has started to increase at a given location since IP_3 diffusion can be viewed as a deterministic process and since the number of puff sites analyzed is large enough. Because puff activity is a stochastic process that also depends on the Ca^{2+} concentration around the cluster, minimal first puff latencies in principle overestimate the time required for IP_3 to spread up to a given location. However, given that minimal first puffs are shorter than 0.5 s at any IP_3 concentration, this delay is anyway small compared to the time needed for IP_3 to spread over distances larger than several microns. Moreover, as discussed below, the minimal first puff latency is not significantly influenced by the possible incomplete Ca^{2+} buffering by EGTA, which could accelerate puff triggering. Indeed, first puffs arise in conditions where most, if not all, nearby clusters are inactive.

Effective diffusion coefficient of IP_3. We investigated the relation between first puff latency and distance from spot photorelease by performing independent simulations for twelve clusters, each one located at a different distance from the photorelease spot in an ellipse-shaped 2D cell. Such a configuration allows to reproduce the absence of communication between the cluster sites that results from the addition of EGTA. Binding of IP_3 to IP_3Rs is taken into account in the value of the effective IP_3 diffusion coefficient, D_I (see Eq. 1). The ellipse shape was chosen instead of the rectangle used in the previous figures to avoid artefactual effects in the corners. Each simulation was run up to the opening of the cluster and this time was then monitored. The same simulation was performed 50 times for each distance between the spot and the cluster. The averages of the latencies of the first puffs correspond to the *mean latencies*. For the *minimal first puff latencies*, we divided the 50 simulations in five groups of ten. In each group, the minimal value was spotted. The average of these minimal values is defined as the minimal first puff latency. As shown in Fig. 4 (upper row), minimal first puffs latencies (black stars) simulated with an effective IP_3 diffusion coefficient of 100 $\mu m^2 s^{-1}$ –which corresponds to the expected value given the IP_3 buffering capacity of the cytosol of SH-SY5Y cells, as discussed in the Introduction– are in agreement with experimental observations of Dickinson et al.[11]. Thus, the time taken by IP_3 to diffuse from the photorelease spot to the locations of the clusters is such that the relation between the distance from the flash spot and the duration of the period of inactivity are well reproduced. Agreement between simulated and observed mean first puff latencies is limited to the case of the 0.1 s flash, *i.e.* the lowest IP_3 concentration. For larger IP_3 concentrations (0.2 and 0.5 s flash), we reasoned that the discrepancy between the idealized simulations of cells containing one single cluster and experiments may be due to a slight stimulation of puff activity by Ca^{2+} in the experiments, which is not totally buffered by EGTA. At 5 µM EGTA, the distance on which free Ca^{2+} ions diffuse before being captured by EGTA is indeed between 2.1 and 3.8 µm (see Sect. 2 of Supplementary Information). As these distances are of the order of the mean distance between clusters in the SH-SY5Y cells, there is some Ca^{2+} stimulation of puff activity in the distributed photorelease protocol. Because we only model one cluster at a time, this effect does not occur in our simulations. Thus, the value $\theta = 600$ $\mu M s^{-1}$ deduced in the previous section overestimates the IP_3 release rate and must be seen as an upper limit.

In line with this assumption, a lower value of parameter θ (250 $\mu M s^{-1}$) representing the rate of IP_3 release due to the flash (Eqs. 3 and 5) allows to get a good agreement both for the mean and the minimal first puff latencies (Fig. 4, medium row). This value of θ also allows us to reproduce the experimentally observed dependency of the mean latency on the flash duration when considering, in the simulations, that the Ca^{2+} level is increased at cluster location during puff activity upon distributed IP_3 photorelease (Supplemental Figure S2). It should be stressed that the 250 $\mu M s^{-1}$ value for θ was found to provide a good fit with observations but remains arbitrary since it cannot be computed on the basis of a detailed quantitative knowledge of the level of communication between the clusters via Ca^{2+}. However, the third row of Fig. 4 shows that agreement with observations cannot be obtained when keeping the large value of θ (600 $\mu M s^{-1}$) and decreasing the value of D_I. In this case, despite the agreement for mean latencies, there is a systematic and important overestimation of the minimal first puff latencies. Such disagreement cannot be ascribed to a reduced number of experimental observations because a larger number of data is only expected to further decrease the shortest possible latency at a given distance. In contrast, it reveals that the low value of D_I is unable to simulate the quite rapid, moderate IP_3 increase away from the spot. The larger concentration of IP_3 due to the overestimated θ explains why mean latencies agree with observations, as they compensate in average for the slow diffusion. Simulations also predict that with $\theta = 250$ $\mu M s^{-1}$ best agreement is obtained with $D_I = 100$ $\mu m^2 s^{-1}$, as compared to smaller or larger values (Fig. 5). Altogether, simulations are in good agreement with experimental observations concerning mean and minimal first puff latencies with the value of the IP_3 diffusion coefficient taking IP_3 binding to the receptors into account, *i.e.* 100 $\mu m^2 s^{-1}$. The

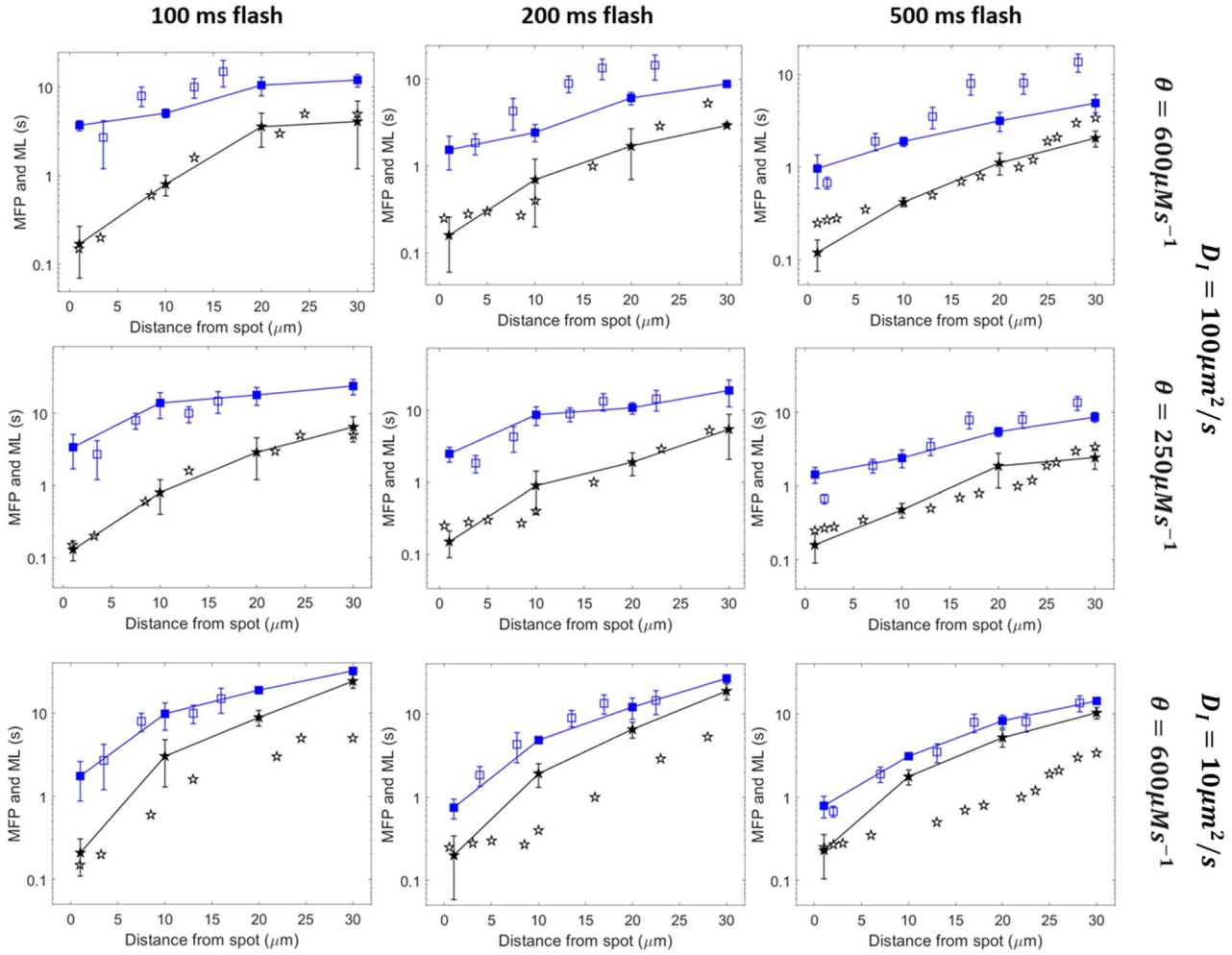

Figure 4. Mean latencies (ML) and minimal first puff latencies (MFP) as simulated with an effective IP_3 diffusion coefficient equal to 100 $\mu m^2 s^{-1}$ (first and second rows) or 10 $\mu m^2 s^{-1}$ (third row) and a rate of IP_3 increase at the photorelease spot of 600 μMs^{-1} (first and third rows) or 250 μMs^{-1} (second row). In all panels, squares represent mean latencies and stars, minimal first puff latencies. Plain symbols are theoretical predictions while empty symbols are the experimental observations of Dickinson et al.[11], estimated from their figures. Lines are drawn between simulation results. Simulations are performed in a 2D ellipse-shaped geometry with the spot of IP_3 release occurring in a 0.25 μm radius circle at one extremity of the simulated cell. For each theoretical point, 50 independent simulations were run, considering one cluster at a time. Error bars indicate ± SEM. For minimal first puffs, the 50 simulations were divided in 10 groups of 5 simulations among which the minimal first puff was considered, except for the case $\theta = 250\ \mu Ms^{-1}$ and the 500 ms flash for which 100 simulations were run for the shortest distance.

latter value also allowed to reproduce the relation between puff latencies and distance from the flash measured in COS-7 cells (Supplemental Figure S3).

Influence of cell shape. Up to this point, simulations have been performed in 2D, rectangular or ellipse-shaped systems. However, the 3D character and the specific geometry of the cells are expected to influence the rate at which IP_3 propagates into the cytoplasm through diffusion. To address this question using computational simulations (Fig. 6), we first considered an ellipsoid (50 × 10 × 5 μm) in which 20 cluster sites are located randomly at a distance shorter than 0.1 μm from the plasma membrane[37]. IP_3 is assumed to be released in a 0.25 μm radius sphere located at the left extremity of the cell. The rate of IP_3 increase (parameter θ in Eqs. 3 and 5) was adapted according to the change in the cytoplasmic volume. Two seconds after the simulated flash, a gradient of IP_3 is established (Fig. 6). Consequently, the dynamics of puff activity is rather different depending on the distance from the flash (compare the Ca^{2+} time series in Fig. 6). Agreement between minimal and mean first puff latencies computed in simulations with an effective diffusion coefficient of IP_3 equal to 100 $\mu m^2 s^{-1}$ and observations of Dickinson et al.[11] is slightly improved in this 3D configuration as compared to the 2D situation (Supplemental Figure S4).

The shape of the cell is expected to influence the rate of IP_3 spreading. We investigated this possible influence by simulating IP_3 diffusion in a two-dimensional representation of an astrocyte (Fig. 7). In response to a release of

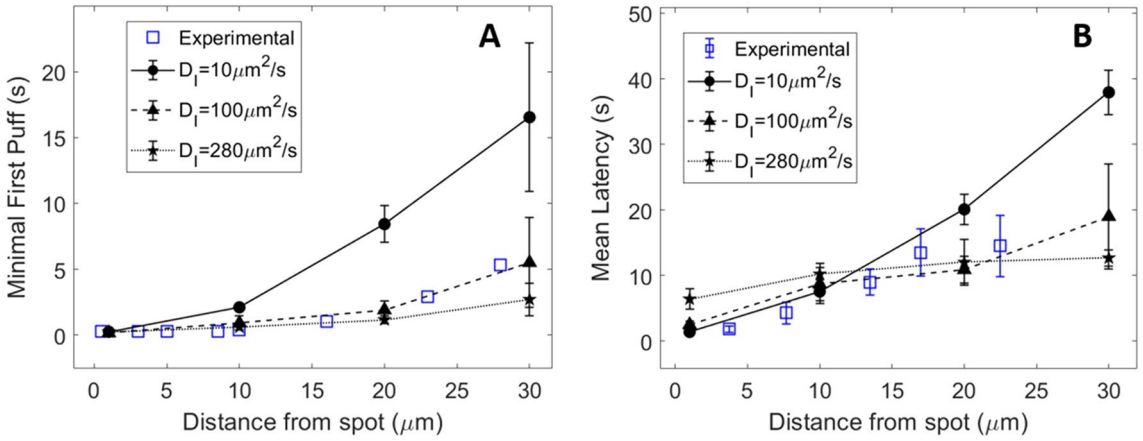

Figure 5. Comparison between puff latencies theoretically predicted with the rate of IP_3 release $\theta = 250$ μm^{2}s^{-1} and observed by Dickinson et al.[11]. Panels (**A and B**) show minimal first puff latencies and mean latencies simulated with different values of the effective diffusion coefficient for IP_3, D_I. All points correspond to a 200 ms flash. Plain symbols are theoretical predictions while empty symbols are the experimental observations of Dickinson et al.[11]. Lines are drawn between simulation results. Simulations are performed in a 2D ellipse-shaped system with the spot of IP_3 release being a 0.25 μm radius disk at one extremity of the simulated cell. For each theoretical point, 50 independent simulations were run. Error bars indicate ± SEM. For minimal first puffs, the 50 simulations were divided in 10 groups of 5 simulations among which the minimal first puff was considered.

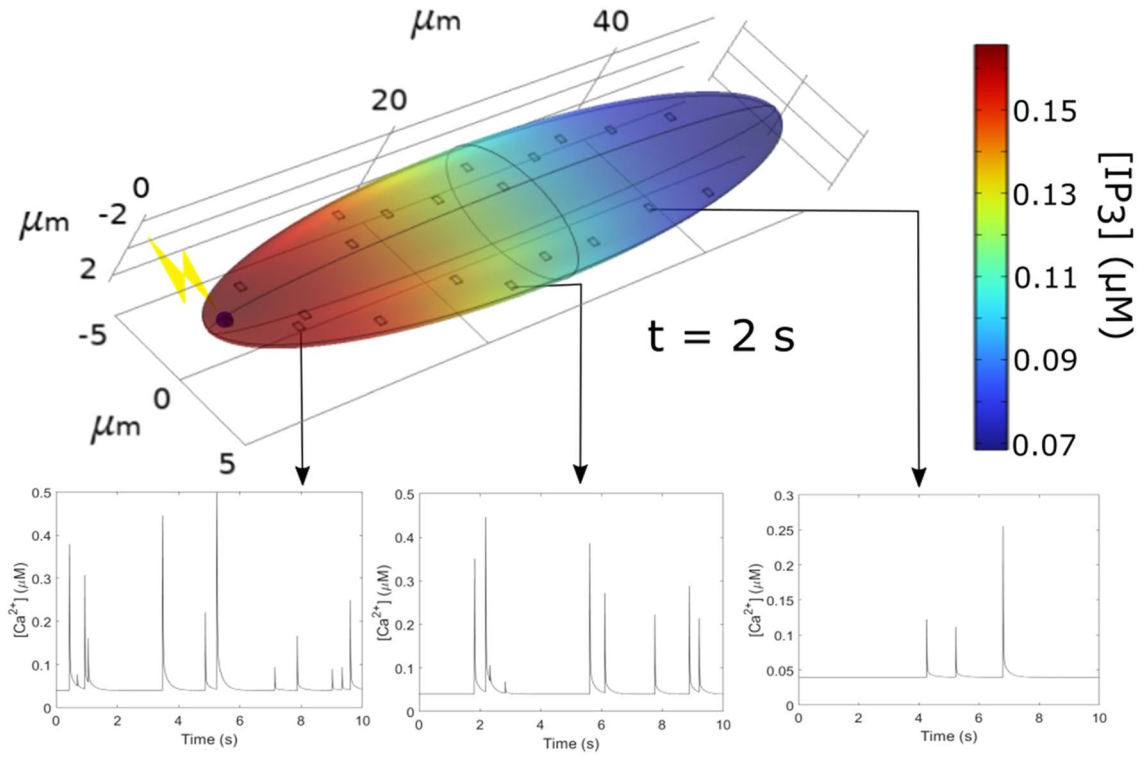

Figure 6. Computational simulations of IP_3 diffusion and Ca^{2+} puff occurrence in response to the localized photorelease of a non-metabolizable IP_3 analogue in an ellipsoidal 3D geometry, assuming an effective diffusion coefficient of IP_3 (D_I) of 100 μm^{2}s^{-1}. The upper panel shows IP_3 distribution 2 s after the flash. Lower panels show time series of local Ca^{2+} concentrations at cluster sites (in a 1 fL volume) located at increasing distances from the flash. Simulation procedures are the same as for Fig. 4. The rate of localized IP_3 photorelease, θ, is taken equal to 2500 μMs^{-1}, which allows to obtain the same spatiotemporal profile of IP_3 increase as the 250 μMs^{-1} value for the 2D case, because of changes in volume.

IP_3 at the intersection between the cell body and one process, Ca^{2+} puffs occur sooner in the cell process than in the body. This is related to a larger rate of IP_3 spreading in elongated structures where dilution is much reduced. For example, 2 s after the simulated flash, more elevated IP_3 concentrations are seen in the process than in the cell body (Fig. 7D). Thus, at the same time and the same distance from the site of IP_3 release, IP_3 reaches higher concentrations in the process and is able to propagate on longer distances (Supplemental Video S5).

In conclusion, the value inferred for the effective IP_3 diffusion coefficient is not significantly affected by considering a 3D system instead of a 2D one. On the other hand, cell shape can considerably affect spreading, with elongated geometries increasing concentration gradients and thereby favoring fast diffusion.

Realistic ER geometry. The ER consists in a network of tubules and flattened sacs, resulting in a complex shape. Since the IP_3 receptors are located within its membrane, spreading of IP_3 to the receptors may be affected by the ER structure. Taking advantage of the great flexibility of Comsol Multiphysics, we performed simulations in which the ER structure was explicitly considered. Thus, we simulated the geometry of a SH-SY5Y cell, in which we inserted an ER whose shape was largely inspired from 2D images of ER in DC-3F cells[39]. We first compared the puff latencies simulated in the absence and in the presence of ER. The values of the rates of IP_3 release were kept the same as in the simulations above (Fig. 4), using a scaling factor to take into account the changes in the cytosolic volume. Puff latencies were in average not much affected by the presence of the ER (Fig. 8). However, the time evolution of the corresponding IP_3 profiles indicates that spreading is locally affected by the extent and the shape of the accessible portions of cytosol between the IP_3 release point and a given puff location. This is most easily visualized in an idealized, ellipse-shaped geometry. In this case, the IP_3 profiles along a fictive line located at half the cell length and perpendicular to the gradient are indeed slightly different when IP_3 is released

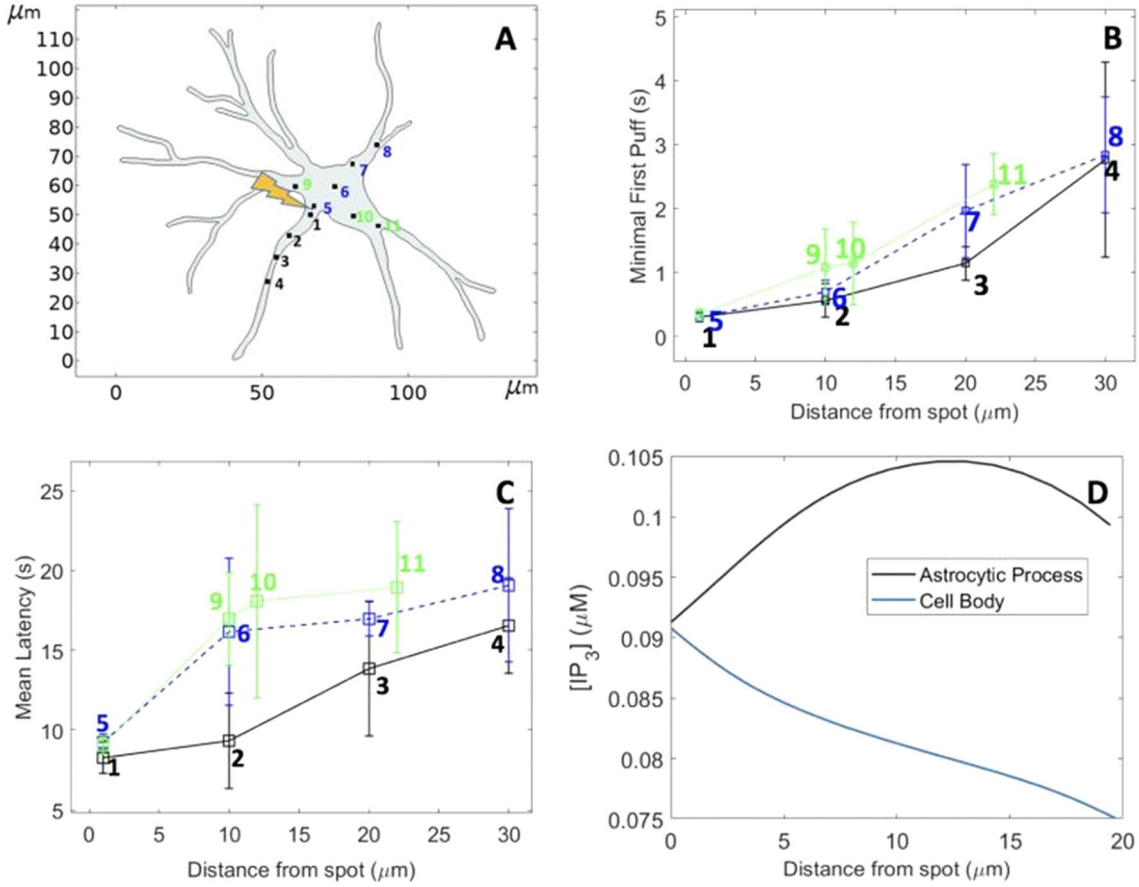

Figure 7. Computational simulations of IP_3 diffusion and Ca^{2+} puff occurrence in response to the localized photorelease of a non-metabolizable IP_3 analogue in a 2D geometry resembling an astrocyte, assuming an effective diffusion coefficient of IP_3 (D_I) of 100 $\mu m^2 s^{-1}$. **(A)** Shape of the astrocyte redrawn in COMSOL Multiphysics from images of Gonçalves-Pimentel et al.[38]. Locations of the clusters considered in the simulations are indicated and labelled in black in the astrocytic process and in blue and green in the cell body. IP_3 photorelease was assumed to occur between locations 1 and 5. Simulation procedures are the same as for Fig. 4 (main text), with $\theta = 250\ \mu m s^{-1}$ and flash duration = 500 ms. Panels **(B and C)** show the minimal first puffs and the mean first puff latencies at the different locations, respectively. At equal distance from the IP_3 release point, puffs occur sooner in the process than in the body. Panel **(D)** shows the distribution of IP_3 2 s after the flash: higher local IP_3 concentrations are reached in the process in which there is no dilution effect. The spatio-temporal evolution of $[IP_3]$ can be seen in the Supplement Video S5.

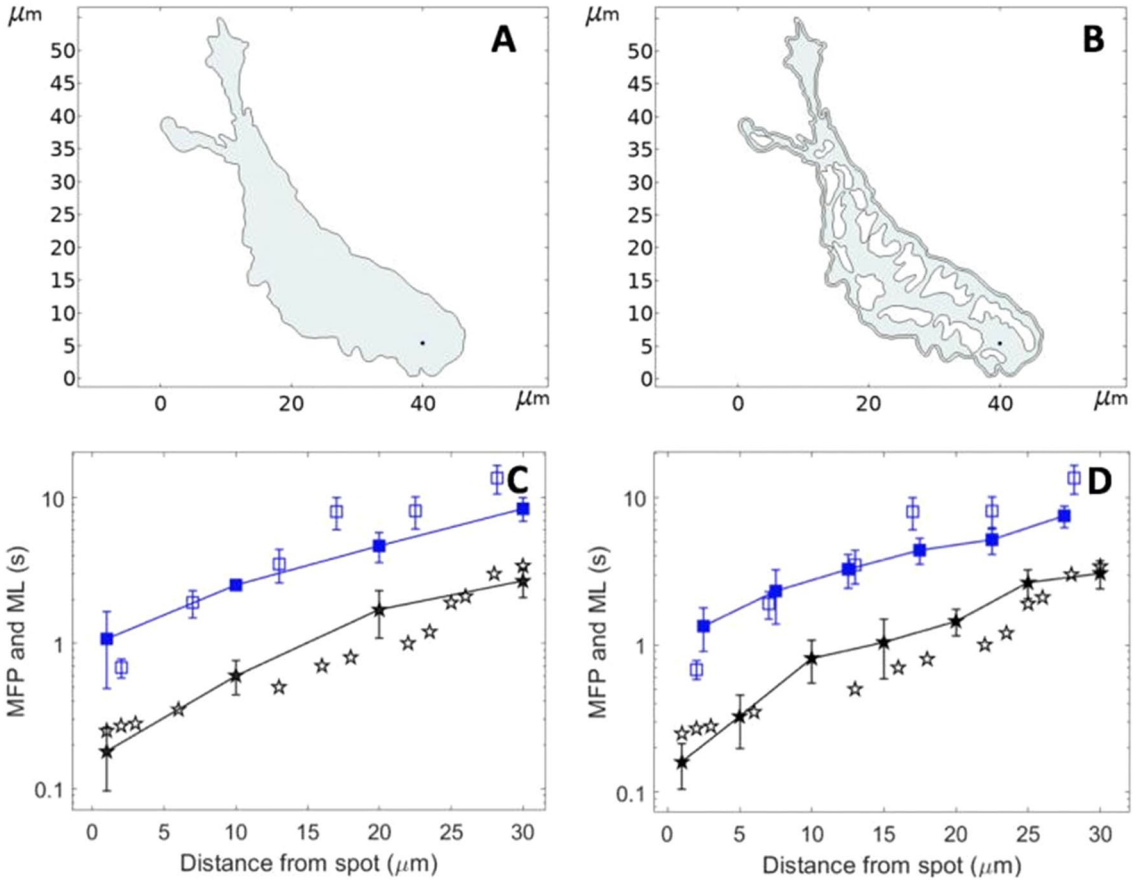

Figure 8. Theoretical investigation of the influence of the ER membranes on the diffusion of IP_3 and Ca^{2+} puff occurrence. Panels (**A and B**) show the 2D geometry considered in the computational simulations of IP_3 diffusion and Ca^{2+} puff occurrence in response to the localized photorelease of a non-metabolizable IP_3 analogue. The shape of the cell was redrawn from Dickinson et al. (2016) and that of the ER was largely inspired from De Angelis et al.[39]. Panels (**C and D**) show the simulated (plain symbols) and experimental (empty symbols) mean latencies (blue) and minimal first puff latencies (black). Flash duration is 500 ms. Simulation procedures are the same as for Fig. 4. The rates of localized IP_3 photorelease, θ, is taken equal to 400.6 μMs^{-1} and 284.65 μMs^{-1}, respectively which corresponds to the 250 μMs^{-1} used in the other simulations with the volumetric adjustments.

at the right or the left extremity of the cell (Fig. 9A–C). Thus, IP_3R clusters locally experience somewhat different IP_3 increases depending on the ER shape, which represents an additional source of randomness in puff activity. When compared to simulations where the ER structure is not considered, average IP_3 increases are in average either a bit slower or similar (Fig. 9D). However, locally, the presence of the ER can also allow for a faster IP_3 increase (Fig. 9B).

In conclusion, simulations indicate that the ER does not much affect average spreading of IP_3 in the cytosol. Although it constitutes a physical barrier that can locally slow down spreading, it also creates cytosolic channel-like structures in which diffusion is accelerated because ions cannot spread in all directions.

Discussion

IP_3 plays a major role in Ca^{2+} signaling by mobilizing Ca^{2+} from the ER, which is the main intracellular Ca^{2+} store. After stimulation, IP_3 must diffuse from the plasma membrane where it is produced across the cytoplasm to trigger Ca^{2+} release from the ER. Thus, IP_3 diffusion plays an essential role in Ca^{2+} signaling. Following measurements in a medium devoid of IP_3R, IP_3 diffusion was assumed to be fast, with a diffusion coefficient[10] of $283 \pm 53\ \mu m^2 s^{-1}$. This estimation is in line with those of compounds of similar molecular weight such as ATP for example[40]. However, this value cannot account for the observation that in response to a localized release of a non-metabolizable analog of IP_3, there is a ~ 10 s delay in the occurrence of Ca^{2+} puffs 30 μm away from the site of IP_3 release[11]. In the same manner, such a rapid diffusion cannot account for the drastic influence of the localization of the IP_3-metabolizing 5-phosphatase enzyme on Ca^{2+} signaling observed in CHO cells by De Smedt et al.[41]. The latter authors developed a mutant $InsP_3$ 5-phosphatase in which the C-terminal cysteine cannot be farnesylated, which hinders its binding to the plasma membrane. While the Ca^{2+} oscillations detected in the presence of 1 μM ATP were totally lost in 87.5% of intact (farnesylated) $InsP_3$ 5-phosphatase-transfected cells, a loss of Ca^{2+} signal occurred in only 1.1% of the mutant $InsP_3$ 5-phosphatase-transfected cells[41]. Such a sensitivity to the location of

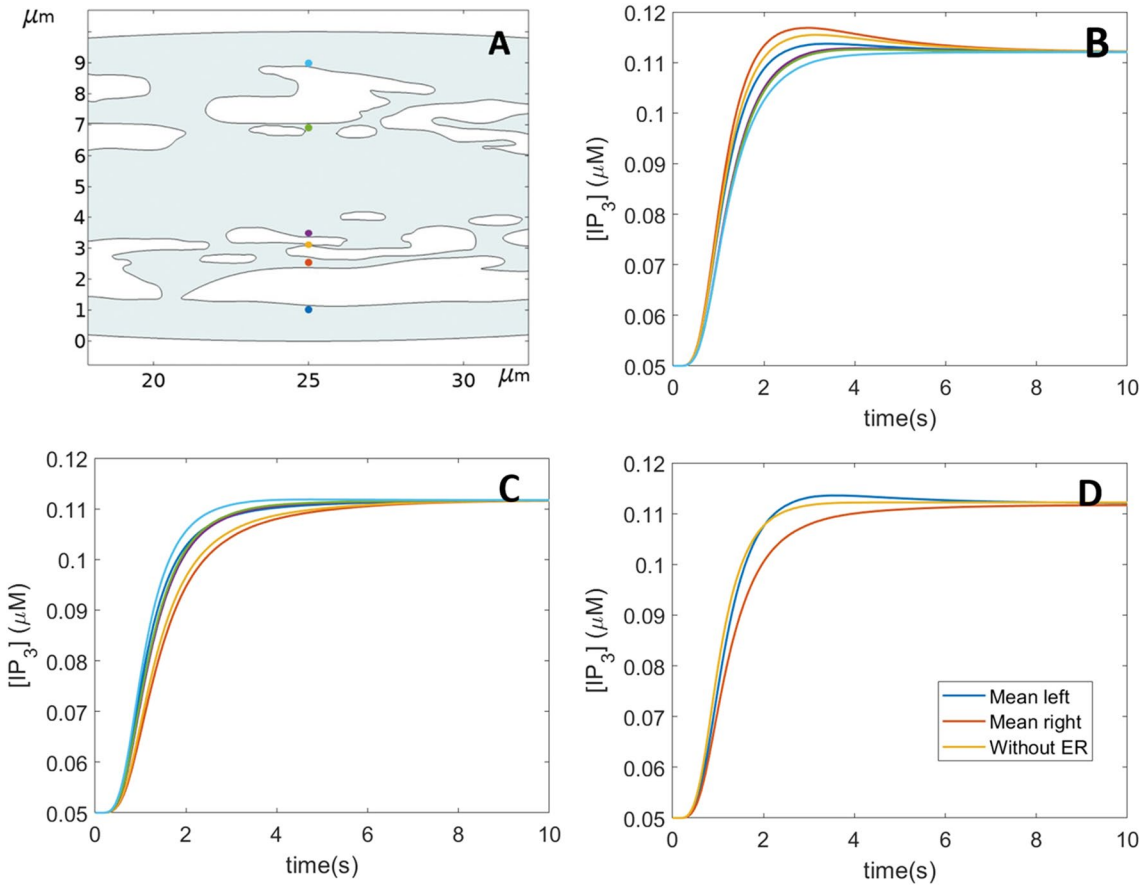

Figure 9. Theoretical investigation of the influence of the ER membranes on the diffusion of IP_3 in a 2D ellipse-shaped cell (50×10 μm^2). Panel (**A**) shows the central part of the simulated cell together with the locations of the clusters considered. Panels (**B and C**) show the IP_3 temporal profiles at the different cluster locations considering a spot of photorelease of IP_3 located at the left (B) or at the right (C) extremity of the cell. Line colors correspond to the points in panel A. In panel (**D**), the profiles of the IP_3 concentrations averaged over the six cluster sites are shown for the two situations corresponding to B and C. Simulation procedures are the same as for Fig. 4. The rate of localized IP_3 photorelease, θ, is taken equal to 179.42 μMs^{-1}, which corresponds to the 250 μMs^{-1} used in the other simulations with the volumetric adjustments.

an IP_3 metabolizing enzyme could not be observed if IP_3 was indeed such a fast-diffusing molecule that rapidly becomes homogeneously distributed in the whole cell.

Accordingly, a much lower value of the effective diffusion coefficient of IP_3 was predicted by Dickinson et al.[11] on the basis of their observations of puff latencies in SH-SY5Y cells in response to the photorelease of a caged non metabolisable IP_3 analog. Although this indirect evaluation of the rate of IP_3 spreading is submitted to uncertainties due to the stochastic nature of Ca^{2+} puffs and to their dependence on Ca^{2+} concentration that is not fully controlled by EGTA, it has the unique advantage of corresponding to realistic cellular conditions. Based on a simplified description of Ca^{2+} puff dynamics, these authors proposed that observations can be accounted for if the effective diffusion coefficient of IP_3 in these cells is in the 3–10 μm^{2}s^{-1} range. This conclusion was re-examined in the present study, based on a detailed description of Ca^{2+} puff dynamics. Our results also point to a lower value of the effective diffusion coefficient of IP_3 in intact cells than in cytosolic extracts of *Xenopus* oocytes but concluded to a decrease by a factor ~ 3 instead of ~ 30. On the basis of their in vitro measurement, Allbritton et al.[10] predicted the range of action of IP_3 to be ~ 24 μm. This is an estimation of the range on which IP_3 can diffuse before being metabolized into another inositol phosphate. Given that this range is proportional to $\sqrt{D_I}$, we would predict a range of action of 14 μm. This value is estimated at 4.5 μm with the D_I value inferred in Dickinson et al.[11]. Since most mammalian cells have a diameter of ~ 12 μm[42], the two values lead to significantly different physiological conclusions. With an effective diffusion coefficient of 100 μm^{2}s^{-1}, IP_3 acts as a global messenger in many cases, although this would not be the case in very large cells such as oocytes or some adipocytes.

Besides the different computational framework, our approach differs from that developed by Dickinson et al. (2016) in three ways. First, only one spatial dimension was considered in the latter study, while we performed 2D or 3D simulations. As illustrated for simulations of IP_3 diffusion in the 1D-like astrocytic process (Fig. 7 and Video S5), diffusion is faster in 1D. The 1D approach of the previous study led to an underestimation of the diffusion coefficient because the value was fitted to reproduce the effective rate of IP_3 diffusion that was observed in 3D. A second important difference relates to the relation between IP_3 concentration and the probability of Ca^{2+} puff occurrence. At low IP_3 concentration, the linear relation considered in the previous study predicts a

larger probability of puff occurrence than the nonlinear function used in the present study (Eq. 2). Again, this higher probability of puff occurrence was compensated by a lower value of the IP_3 diffusion coefficient. Thirdly, because we here considered both the mean and the minimal first puff latencies, we inferred the rate of IP_3 release by the flash (parameter θ in Eqs. 3 and 5) in a more accurate way. We reasoned that the mean first puff latency is affected by an increase in Ca^{2+} because the latter is not fully prevented by the EGTA injected in the cell at a final concentration of 5 µM. In line with this hypothesis, agreement for both mean and first puff latencies was only obtained in our simulations when considering that locally the level of Ca^{2+} was in average 120 nM above basal level when puff activity was monitored after distributed photorelease of IP_3. Because this Ca^{2+} increase was not taken into account in the previous study of Dickinson et al.[11], the value of θ was overestimated, leading again to an underestimation of the IP_3 diffusion coefficient.

To confirm that the IP_3 diffusion coefficient is indeed larger than 10 $\mu m^2 s^{-1}$, we simulated the experimental protocol of distributed photorelease of IP_3 used in Dickinson et al.[11] to induce a spatially uniform rise in IP_3 concentration and described in the methodology section here above. Simulations performed with $D_I = 10\ \mu m^2 s^{-1}$ and shown in Figure S6B&D show that IP_3 concentration remains spatially inhomogeneous up to at least 10 s after the flash. This is not in agreement with the observation that first puff latencies are independent from the distance from cell end under this protocol. In contrast, when $D_I = 100\ \mu m^2 s^{-1}$, IP_3 rapidly equilibrates in the whole cell (Figure S6C).

Simulations predict that IP_3 spreading is not much affected by the proximity of the plasma membrane. Indeed, times of puffs occurrence are mainly determined by the distance of the clusters from the spot of IP_3 photorelease and not by their positions in the bulk of the cytoplasm (as in Fig. 4) or close to the plasma membrane (as in Fig. 6). This is relevant because clusters of IP_3 receptors are most of the time located very close to the plasma membrane[37]. Similarly, IP_3 spreading is not much affected by the precise shape of the cell. Simulations of puff activity indeed lead to similar results in a 2D ellipse-shaped cell (Fig. 4), in a 3D ellipsoid (Fig. 6) or in a 2D configuration resembling a SH-SY5Y cell (Fig. 8). However, elongated geometries favor fast diffusion and allow for higher local [IP_3] than in extended systems. This was shown here by simulations in a situation corresponding to an astrocyte. Accordingly, rates of Ca^{2+} waves propagation in astrocytic processes are larger than in most cell types (33–100 μms^{-1}, see Cornell-Bell and Finkbeiner[43] versus 10–20 μms^{-1}, see Dupont et al.[23]). Surprisingly, the presence of the ER, which acts as an obstacle to free diffusion, does not much affect mean effective diffusion. This lack of global effect can be ascribed to the fact that while some paths are slower because of obstruction, others are faster because of the presence of channel-like structures which favor fast diffusion thanks to the absence of dilution effect. It should be noted that we did not consider the tubular-shaped of this network, nor its dynamical evolution into a more fragmented structure[44].

The value of 100 $\mu m^2 s^{-1}$ for the effective diffusion coefficient of IP_3 that emerges from our simulations is in line with the buffering effect exerted by the non-fully bound IP_3R tetramers, as proposed previously[11,13]. Thus, it is expected to be smaller in cell types with higher expression levels of IP_3R. In the same line, effective diffusion is much accelerated upon increasing [IP_3] because buffers become saturated. Thus, upon cell stimulation by an agonist that generally leads to a surge in [IP_3] followed by a decrease, the properties of diffusion are expected to vary. Even more significant in this respect are the IP_3 oscillations that have been observed in several cell types and that arise from the activation by Ca^{2+} of IP_3 synthesis by PLC[45] and/or of IP_3 metabolism by a 3-kinase[46,47]. Further studies are required to assess the consequences of the interplay between the temporal changes in IP_3 concentration and its diffusional properties.

Data availability

Codes are available at https://github.com/RobertoOrnelasGuevara/ca2-puffs/tree/main.

Received: 30 September 2022; Accepted: 11 February 2023
Published online: 20 February 2023

References

1. Bootman, M. *et al.* Calcium signalling – an overview. *Seminar Cell Dev. Biol.* **12**, 3–10 (2001).
2. Berridge, M. J. Elementary and global aspects of calcium signalling. *J. Physiol.* **499**, 291–306 (1997).
3. Sammels, E., Parys, J., Missiaen, L., De Smedt, H. & Bultynck, G. Intracellular Ca^{2+} storage in health and disease: a dynamic equilibrium. *Cell Calcium* **47**, 297–314 (2010).
4. Bezprozvanny, I., Watras, J. & Ehrlich, B. Bell-shaped calcium-response curves of $Ins(1,4,5)P_3$- and calcium-gated channels from endoplasmic reticulum of cerebellum. *Nature* **351**, 751–754 (1991).
5. Smith, I. & Parker, I. Imaging the quantal substructure of single IP_3R channel activity during Ca^{2+} puffs in intact mammalian cells. *Proc. Natl. Acad. Sci. USA* **106**, 6404–6409 (2009).
6. Swillens, S., Dupont, G., Combettes, L. & Champeil, P. From calcium blips to calcium puffs: theoretical analysis of the requirements for interchannel communication. *Proc. Natl. Acad. Sci. USA* **96**, 13750–13755 (1999).
7. Bootman, M., Berridge, M. & Lipp, P. Cooking with calcium: The recipes for composing global signals from elementary events. *Cell* **91**, 367–373 (1997).
8. Skupin, A. *et al.* How does intracellular Ca^{2+} oscillate: By chance or by the clock?. *Biophys. J.* **94**, 2404–2411 (2008).
9. Voorsluijs, V., Ponce Dawson, S., De Decker, Y. & Dupont, G. Deterministic limit of intracellular calcium spikes. *Phys. Rev. Lett.* **122**, 088101 (2019).
10. Allbritton, N., Meyer, T. & Stryer, L. Range of messenger action of calcium ion and inositol 1,4,5-trisphosphate. *Science* **258**, 1812–1815 (1992).
11. Dickinson, G., Ellefsen, K., Ponce Dawson, S., Pearson, J. & Parker, I. Hindered cytoplasmic diffusion of inositol trisphosphate restricts its cellular range of action. *Sci. Signal.* **9**, ra108 (2016).
12. Yao, Y., Choi, I. & Parker, I. Quantal puffs of intracellular Ca^{2+} evoked by inositol trisphosphate in *Xenopus* oocytes. *J. Physiol.* **482**, 533–553 (1995).
13. Taylor, C. & Konieczny, V. IP_3 receptors: Take four IP_3 to open. *Science Signaling* **9**(422):pe1 (2016)

14. Alzayady, K. *et al.* Defining the stoichiometry of inositol 1,4,5-trisphosphate binding required to initiate Ca^{2+} release. *Science Signaling* **9**(422), ra35 (2016).
15. Dupont, G., Falcke, M., Kirk, V. & Sneyd, J. Models of calcium signalling. Interdisciplinary Applied Mathematics (Springer International Publishing, Switzerland), Vol 43. (2016)
16. Dupont, G., Abou-Lovergne, A. & Combettes, L. Stochastic aspects of oscillatory Ca^{2+} dynamics in hepatocytes. *Biophys. J.* **95**, 2193–2202 (2008).
17. Spät, A., Bradford, P., McKinney, J., Rubin, R. & Putney, J. A saturable receptor for ^{32}P-inositol-1,4,5-trisphosphate in hepatocytes and neutrophils. *Nature* **319**, 514–516 (1986).
18. Wojcikiewicz, R. Type I, II, and III inositol 1,4,5-trisphosphate receptors are unequally susceptible to down-regulation and are expressed in markedly different proportions in different cell types. *J. Biol. Chem.* **270**, 11678–11683 (1995).
19. Tanimura, A. *et al.* Use of fluorescence resonance energy tansfer-based biosensors for the quantitative analysis of inositol 1,4,5-trisphosphate dynamics in calcium oscillations. *J. Biol. Chem.* **284**, 8910–8917 (2009).
20. Lock, J. & Parker, I. IP_3 mediated global Ca^{2+} signals arise through two temporally and spatially distinct modes of Ca^{2+} release. *eLife* **9:** e55008 (2020)
21. Dupont, G. & Dumollard, R. Simulation of calcium waves in ascidian eggs: insights into the origin of the pacemaker sites and the possible nature of the sperm factor. *J. Cell Sci.* **117**, 4313–4323 (2004).
22. Decrock, E. *et al.* IP_3, a small molecule with a powerful message. *Biochim. Biophys. Acta* **1833**, 1772–1786 (2013).
23. Dupont, G., Combettes, L. & Leybaert, L. Calcium dynamics: spatio-temporal organization from the subcellular to the organ level. *Int. Rev. Cytol.* **261**, 193–245 (2007).
24. Leybaert, L. IP_3, still on the move but now in the slow lane. *Sci. Signal.* **9**, fs17 (2016).
25. Pawar, A. & Pardasani, K. Effects of disorders in interdependent calcium and IP_3 dynamics on nitric oxide production in a neuron cell. *Eur. Phys. Journ. Plus* **137**, 543 (2022).
26. Pawar, A., Pardasani, K. Effects of disturbances in neuronal calcium and IP_3 dynamics on b-amyloid production and degradation. *Cognitive Neurodyn.* https://doi.org/10.1007/s11571-022-09815-0 (2022)
27. Sneyd, J. *et al.* Modeling calcium waves in an anatomically accurate three-dimensional parotid acinar cells. *J. Theor. Biol.* **419**, 383–393 (2017).
28. Hohendanner, F., McCulloch, A., Blatter, L. & Michailova, A. Calcium and IP_3 dynamics in cardiac myocytes: experimental and computational perspectives and approaches. *Front. Pharmacol.* **10**, 3389 (2014).
29. Singh, N. & Adlakha, N. A mathematical model for interdependent calcium and inositol 1,4,5-trisphosphate in cardiac myocyte. *Netw. Model. Anal. Health Informat. Bioinformat.* **8**, 18 (2019).
30. Gillespie, D. A general method for numerically simulating the stochastic time evolution of coupled chemical reactions. *J. Comput. Phys.* **22**, 403–434 (1976).
31. Calabrese, A., Fraiman, D., Zysman, D. & Ponce Dawson, S. Stochastic fire-diffuse-fire model with realistic cluster dynamics. *Phys. Rev. E* **82**, 031910 (2010).
32. Dickinson, G., Swaminathan, D. & Parker, I. The probability of triggering calcium puffs is linearly related to the number of inositol trisphosphate receptors in a cluster. *Biophys. J.* **102**, 1826–1836 (2012).
33. Luzzi, V., Sims, C., Soughayer, J. & Allbritton, N. The physiological concentration of inositol 1,4,5-trisphosphate in the oocytes of *Xenopus laevis*. *J. Biol. Chem.* **273**, 28657–28662 (1998).
34. Tovey, S. *et al.* Calcium puffs are generic $InsP_3$-activated elementary calcium signals and are downregulated by prolonged hormonal stimulation to inhibit cellular calcium responses. *J. Cell Sci.* **114**, 3979–3989 (2001).
35. Thurley, K., Tovey, S., Moenke, G., Prince, V., Meena, A., Thomas, A., Skupin, A., Taylor, C. & Falcke, M. Reliable encoding of stimulus intensities with random sequences of intracellular Ca^{2+} spikes. *Sci. Signal.* **7(331)**: ra59 (2014)
36. Dargan, S. & Parker, I. Buffer kinetics shape the spatiotemporal patterns of IP_3-evoked Ca^{2+} signals. *J. Physiol.* **553**, 775–788 (2003).
37. Smith, I., Wiltgen, S. & Parker, I. Localization of puff sites adjacent to the plasma membrane: functional and spatial characterization of Ca^{2+} signaling in SH-SY5Y cells utilizing membrane-permeant caged IP_3. *Cell Calcium* **45**, 65–76 (2009).
38. Gonçalves-Pimentel, C. *et al.* Cellulose exopolysaccharide from sugarcane molasses as a suitable substrate for 2D and 3D neuron and astrocyte primary cultures. *J. Mater. Sci. Mater. Med.* **29**, 139 (2018).
39. De Angelis, A. *et al.* Microdosimetric realistic model of a cell with endoplasmic reticulum. *Ann. Int. Conf. IEEE Eng. Med. Biol. Soc.* **2019**, 134–137 (2019).
40. Hubley, M., Moerland, T. & Rosanke, R. Diffusion coefficient of ATP and creatine phosphate in isolated muscle: pulsed gradient ^{31}P NMR of small biological sample. *NMR Biomed.* **8**, 72–78 (1995).
41. De Smedt, F. *et al.* Isoprenylated human brain type I inositol 1,4,5-trisphosphate 5-phosphatase controls Ca^{2+} oscillations induced by ATP in Chinese hamster ovary cells. *J. Biol. Chem.* **272**, 17367–17375 (1997).
42. Milo, R. & Phillips, R. *Cell biology by the numbers* (CRC Press, 2015).
43. Cornell-Bell, A. & Finkbeiner, S. Ca^{2+} waves in astrocytes. *Cell Calcium* **12**, 185–204 (1991).
44. Subramanian, K. & Meyer, T. Calcium-induced restructuring of nuclear envelope and endoplasmic reticulum calcium stores. *Cell* **89**, 963–971 (1997).
45. Politi, A., Gaspers, L., Thomas, A. & Höfer, T. Models of IP_3 and Ca^{2+} oscillations: frequency encoding and identification of underlying feedbacks. *Biophys. J.* **90**, 3120–3133 (2006).
46. Dupont, G. & Erneux, C. Simulations of the effects of inositol 1,4,5-trisphosphate 3-kinase and 5-phosphatase activities on Ca^{2+} oscillations. *Cell Calcium* **22**, 321–331 (1997).
47. Sneyd, J. *et al.* (2006) A method for determining the dependence of calcium oscillations on inositol trisphosphate oscillations. *Proc. Natl. Acad. Sci. USA* **103**, 1675–1680 (2006).

Acknowledgements

This work was supported by a PDR FRS-FNRS project (T.0073.21). GD is Research Director at the Belgian "Fonds National pour la Recherche Scientifique" (FRS-FNRS). We thank Benjamin Wacquier and Laurent Combettes for scientific help and fruitful discussions, as well as Silvina Ponce Dawson for constructive comments.

Author contributions

Conceptualization by ROG and GD. Code development by ROG, VV and DG. Analysis of the simulations by all authors. Writing of original draft by GD and ROG. Editing by all others.

Competing interests

The authors declare no competing interests.

Additional information

Supplementary Information The online version contains supplementary material available at https://doi.org/10.1038/s41598-023-29876-3.

Correspondence and requests for materials should be addressed to G.D.

Reprints and permissions information is available at www.nature.com/reprints.

Publisher's note Springer Nature remains neutral with regard to jurisdictional claims in published maps and institutional affiliations.